Atom-Efficient Catalytic Coupling of Imidazolium Salts with Ethylene Involving Ni−NHC Complexes as Intermediates: A Combined Experimental and DFT Study

Adrien T. Normand,[†] Kirsty J. Hawkes,[†,‡] Nicolas D. Clement,[†,§] Kingsley J. Cavell,*[,†] and Brian F. Yates*[,‡]

School of Chemistry, Main Building, Cardiff University, Park Place, Cardiff, Wales, U.K. CF10 3AT, and School of Chemistry, University of Tasmania, GPO Box 252-75, Hobart, Tasmania 7001, Australia

Received February 27, 2007

The coupling reaction between azolium salts (N-heterocyclic carbene precursors) and ethylene, catalyzed by zerovalent nickel complexes, has been investigated using a combination of experiment and density functional theory (DFT). The reaction proceeds via a redox mechanism involving the generation of Ni−carbene intermediates. The experimental studies employed an in situ catalyst system, derived from Ni(COD)$_2$ and a variety of phosphine and N-heterocyclic carbene spectator ligands, to couple 1-propyl-3-methylimidazolium bromide (ionic liquid) and other azolium salts with ethylene. The DFT studies employed the simpler dimethylimidazolium salt to model the reaction.

Introduction

N-heterocyclic carbenes (NHCs; Figure 1) are regarded as very effective ligands for homogeneous catalysis, and they often lead to high efficiencies in metal-catalyzed reactions when contrasted with the more traditional phosphines,[1,2] with which they are frequently compared.

While in general NHC complexes are considered to be very stable species, due to their unique electronic properties and the high bond dissociation energies (BDE) of NHCs,[3] previous work in our group has shown that Pd− and Ni−hydrocarbyl complexes of NHCs readily decompose by reductive elimination to yield 2-substituted imidazolium salts.[4−7] In addition, NHC complexes of other late transition metals sometimes show unexpected reactivities.[8−14] Subsequent studies demonstrated that the "reverse" reaction (i.e. oxidative addition of imidazolium salts to zerovalent group 10 metals) is also possible.[6,15−19] A feature of this oxidative addition chemistry is the use of what is effectively an imidazolium-based ionic liquid, to directly form metal carbene hydride complexes. Metal hydrides are believed to be the active species in a variety of catalytic reactions.[20−24] We first isolated carbene−metal−hydride complexes with Pt[18,25] and then subsequently with Ni and Pd (Scheme 1).[6,17]

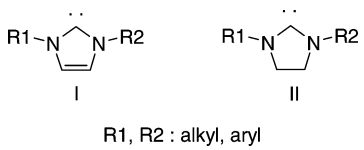

Figure 1. Saturated (I) and unsaturated (II) N-heterocyclic carbenes.

In more recent studies we have combined these redox reactions to generate an atom-efficient coupling reaction between azolium salts and alkenes (Scheme 2)[19] and, in turn, to

* To whom correspondence should be addressed. E-mail: cavellkj@cf.ac.uk (K.J.C.); Brian.Yates@utas.edu.au (B.F.Y.).
† Cardiff University.
‡ University of Tasmania.
§ Current address: Leibniz-Institüt für Katalyse e.V. an der Universität Rostock, Albert-Einstein-Str. 29a, D-18059 Rostock, Germany

(1) Bourissou, D.; Guerret, O.; Gabbai, F. P.; Bertrand, G. *Chem. Rev.* **2000**, *100*, 39−91.
(2) Herrmann, W. A. *Angew. Chem., Int. Ed.* **2002**, *41*, 1290−1309.
(3) Crudden, C. M.; Allen, D. P. *Coord. Chem. Rev.* **2004**, *248*, 2247−2273.
(4) McGuinness, D. S.; Saendig, N.; Yates, B. F.; Cavell, K. J. *J. Am. Chem. Soc.* **2001**, *123*, 4029−4040.
(5) Cavell, K. J.; McGuinness, D. S. *Coord. Chem. Rev.* **2004**, *248*, 671−679.
(6) Bacciu, D.; Cavell, K. J.; Fallis, I. A.; Ooi, L.-l. *Angew. Chem., Int. Ed.* **2005**, *44*, 5282−5284.
(7) Graham, D. C.; Cavell, K. J.; Yates, B. F. *Dalton Trans.* **2005**, 1093−1100.
(8) Jazzar, R. F. R.; Macgregor, S. A.; Mahon, M. F.; Richards, S. P.; Whittlesey, M. K. *J. Am. Chem. Soc.* **2002**, *124*, 4944−4945.
(9) Chilvers, M. J.; Jazzar, R. F. R.; Mahon, M. F.; Whittlesey, M. K. *Adv. Synth. Catal.* **2003**, *345*, 1111−1114.
(10) Burling, S.; Mahon, M. F.; Paine, B. M.; Whittlesey, M. K.; Williams, J. M. J. *Organometallics* **2004**, *23*, 4537−4539.
(11) Caddick, S.; Cloke, G. N.; Hitchcock, P. B.; Lewis, A. K. d. K. *Angew. Chem., Int. Ed.* **2004**, *43*, 5824−5827.
(12) Ampt, K. A. M.; Burling, S.; Donald, S. M. A.; Douglas, S.; Duckett, S. B.; Macgregor, S. A.; Perutz, R. N.; Whittlesey, M. K. *J. Am. Chem. Soc.* **2006**, *128*, 7452−7453.
(13) Burling, S.; Mahon, M. F.; Powell, R. E.; Whittlesey, M. K.; Williams, J. M. J. *J. Am. Chem. Soc.* **2006**, *128*, 13702−13703.
(14) Diggle, R. A.; Macgregor, S. A.; Whittlesey, M. K. *Organometallics* **2004**, *23*, 1857−1865.
(15) McGuinness, D. S.; Cavell, K. J.; Yates, B. F.; Skelton, B. W.; White, A. H. *J. Am. Chem. Soc.* **2001**, *123*, 8317−8328.
(16) Hawkes, K. J.; McGuinness, D. S.; Cavell, K. J.; Yates, B. F. *Dalton Trans.* **2004**, 2505−2513.
(17) Clement, N. D.; Cavell, K. J.; Jones, C.; Elsevier, C. J. *Angew. Chem., Int. Ed.* **2004**, *43*, 1277−1279.
(18) McGuinness, D. S.; Cavell, K. J.; Yates, B. F. *Chem. Commun.* **2001**, 355−356.
(19) Clement, N. D.; Cavell, K. J. *Angew. Chem., Int. Ed.* **2004**, *43*, 3845−3847.
(20) Van Leeuwen, P. W. N. M. *Homogeneous Catalysis*; Kluwer Academic: Dordrecht, The Netherlands, 2004.
(21) Crabtree, R. H. *The Organometallic Chemistry of the Transition Metals*, 3rd ed.; Wiley: New York, 2000.
(22) Hills, I. D.; Fu, G. C. *J. Am. Chem. Soc.* **2004**, *126*, 13178−13179.
(23) Nguyen, D. H.; Laurenczy, G.; Urrutigoïty, M.; Calck, P. *Eur. J. Inorg. Chem.* **2005**, 4215−4225.
(24) Grushin, V. V. *Chem. Rev.* **1996**, *96*, 2011−2033.
(25) Duin, M. A.; Clement, N. D.; Cavell, K. J.; Elsevier, C. J. *Chem. Commun.* **2003**, 400−401.

10.1021/om070181e CCC: $37.00
Publication on Web 09/29/2007

Scheme 1. Metal Hydrides Obtained from Oxidative Addition to Imidazolium Salts

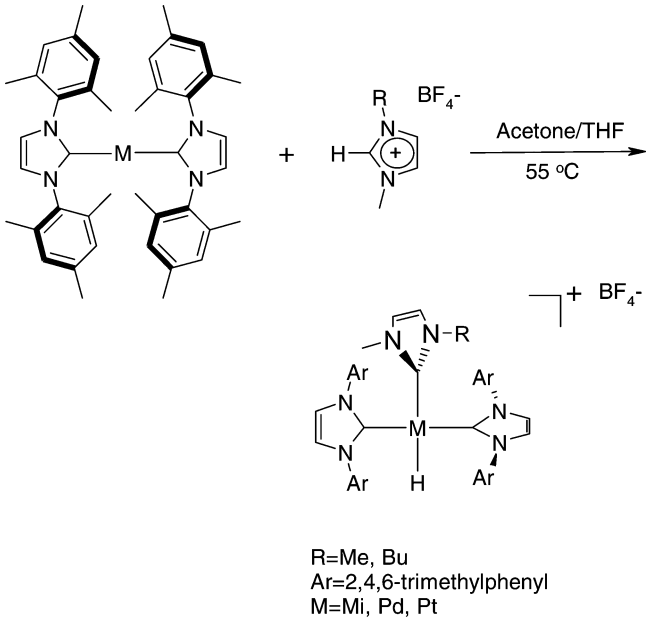

R=Me, Bu
Ar=2,4,6-trimethylphenyl
M=Mi, Pd, Pt

Scheme 2. Reaction of Olefins with *N*-Alkyl Azolium Salts

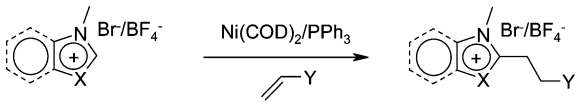

X=O, S, NR'
R=alkyl
Y=H, Ph, C_4H_9

Scheme 3. Functionalization of Heterocyclic Substrates via Transition Metals

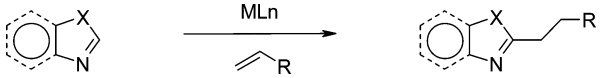

demonstrate the in situ formation of reactive metal−hydride complexes. A range of olefins were successfully coupled to give the 2-substituted product.[12]

With the current interest in ionic liquids (ILs) based on imidazolium salts as "green" media for chemical reactions,[26−30] this reaction provides a useful, modular approach to the synthesis of finely tuned ILs, using simple imidazolium salts as building blocks. An important extension of this work is the C2 functionalization of imidazoles and related heterocycles (Scheme 3).[31−36] Elegant work by Bergman has shown that these species

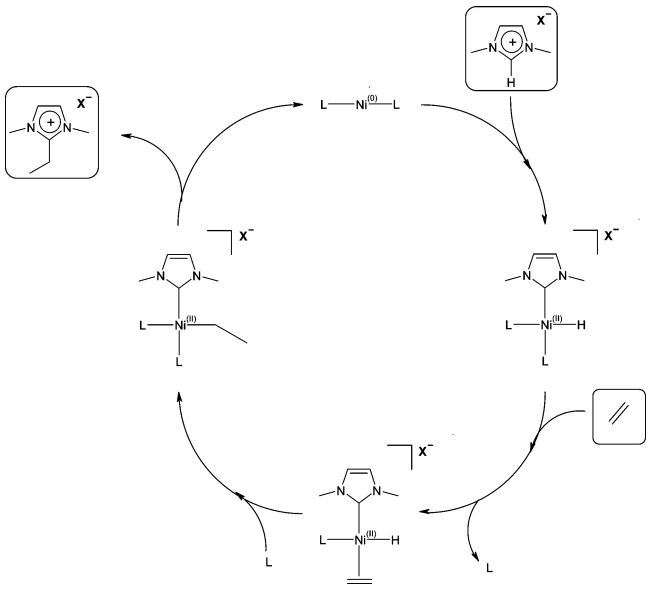

Figure 2. Proposed "redox" mechanism for the reaction of olefins with imidazolium salts.

can be successfully reacted with olefins in the presence of a rhodium catalyst via an NHC intermediate.[35,37] This methodology has now been applied to the total synthesis of biologically active compounds.[38] With increasing pressure on chemists to develop cleaner, atom-efficient reactions, direct functionalization of C−H bonds is becoming a strategically important area of chemistry. In this context, our previously reported olefin/azolium salt coupling reaction bears considerable potential, and we felt it was important to better understand and broaden the scope of this unique process.

We previously proposed that the catalytic cycle using the catalyst system $Ni(COD)_2/PPh_3$ proceeds via a mechanism involving oxidative addition of the azolium salt and replacement of a weakly bound ligand by alkene, followed by insertion of the alkene into the metal−hydride bond and, finally, reductive elimination of the product ("redox" mechanism; Figure 2),[19] Therefore, in order to optimize and extend this new catalytic process, we now report a combined experimental and computational study that describes how this mechanism might be modified, contingent on the nature of the ancillary ligand. Investigations reveal how changes in electronic and steric properties of the ligand dramatically influence the outcome of the reaction. We describe the coupling reaction for a range of azolium salts and alkenes and for a range of catalyst systems. The reaction of a benzothiazole to form a 2-substituted benzothiazole is reported, thus broadening the reaction to include neutral azoles. We also describe a detailed computational investigation of the reaction mechanism focusing specifically on the coupling of ethylene and 1,3-dimethylimidazolium, with a range of NiL_1L_2 catalyst systems.

Experimental Study

Substrate Range. The reaction of ethylene with a variety of azolium salts was investigated with a view to determining a cross-section of substrates that will undergo this coupling

(26) Sheldon, R. *Chem. Commun.* **2001**, 2399−2407.
(27) Wasserscheid, P.; Keim, W. *Angew. Chem., Int. Ed.* **2000**, *39*, 3772−3789.
(28) Chiappe, C.; Pieraccini, D. *J. Phys. Org. Chem.* **2005**, *18*, 275−297.
(29) Jain, N.; Kumar, A.; Chauhan, S.; Chauhan, S. M. S. *Tetrahedron* **2005**, *61*, 1015−1060.
(30) Zeitler, K. *Angew. Chem., Int. Ed.* **2005**, *44*, 7506−7510.
(31) Tan, K. L.; Ellman, J. A.; Bergman, R. G. *J. Org. Chem.* **2004**, *69*, 7329−7335.
(32) Thalji, R. K.; Ahrendt, K. A.; Bergman, R. G.; Ellman, J. A. *J. Org. Chem.* **2005**, *70*, 6775−6781.
(33) Lewis, J. C.; Wiedemann, S. H.; Bergman, R. G.; Ellman, J. A. *Org. Lett.* **2004**, *6*, 35−38.
(34) Tan, K. L.; Bergman, R. G.; Ellman, J. A. *J. Am. Chem. Soc.* **2002**, *124*, 13964−13965.
(35) Tan, K. L.; Bergman, R. G.; Ellman, J. A. *J. Am. Chem. Soc.* **2002**, *124*, 3202−3203.
(36) Wiedemann, S. H.; Bergman, R. G.; Ellman, J. A. *Org. Lett.* **2004**, *6*, 1685−1687.
(37) Wiedemann, S. H.; Lewis, J. C.; Ellman, J. A.; Bergman, R. G. *J. Am. Chem. Soc.* **2006**, *128*, 2452−2462.
(38) Wiedemann, S. H.; Ellman, J. A.; Bergman, R. G. *J. Org. Chem.* **2006**, *71*, 1969−1976.

Table 1. Functionalization of Azolium Salts[a]

Entry	Azolium salt	product	Conv (%)[b]
1	**1a**	**1b**	100
2	**2a**	**2b**	100
3	**3a**	**3b**	100
4	**4a**	**4b**	100
5	**5a**	**5b**	100

[a] Reagents and conditions: azolium salt, 0.73 mmol; ethylene, 1 bar; $Ni(COD)_2$, 10 mol %; PPh_3, 21 mol %; acetone−THF (3:1), 12 mL; 55 °C; 48 h. [b] Determined by ^1H NMR spectroscopy: average of two runs or more.

Table 2. C2 Functionalization of BF_3-Activated Benzothiazole[a]

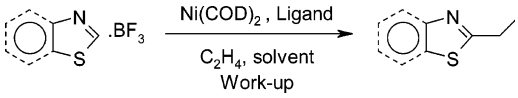

entry	ligand (equiv/Ni)	solvent	Conv (%)[b]
1	PCy_3 (2.1)	BTF[c]	25
2	PCy_3 (1.1)	BTF	0
3	IMes (2.1)	BTF	0
4	PMe_2Ph (2.1)	BTF	28
5	PMe_2Ph (2.1)	toluene	50

[a] Reagents and conditions: adduct, 0.73 mmol; $Ni(COD)_2$, 10 mol %; solvent, 3 mL; ethylene, 1 bar; 80 °C; 24 h; entries 1−3, one run; entry 4, two runs; entry 5, four runs. [b] Determined by GCMS. [c] α,α,α-Trifluorotoluene.

reaction. Results in Table 1 indicate that the reaction can be applied to a large range of azolium salts: e.g., thiazolium (**1a**), benzothiazolium (**2a**), oxazolium (**3a**), benzoxazolium (**4a**), and 1,3-dimethyltriazolium (**5a**). High yields of 2-substituted product are consistently obtained (Table 1). Interestingly, the triazolium salt **5a** formed the doubly substituted product **5b**. New compounds were characterized by NMR, electrospray mass spectrometry, and microanalysis.[39]

To further demonstrate the extent of the reaction, the neutral heterocycle benzothiazole was also substituted in the 2-position using this methodology (Table 2). However, it was necessary to use a Lewis acid (e.g., BF_3−etherate) to sufficiently activate the azole and give a satisfactory yield of product. The benzothiazole−boron trifluoride adduct could be prepared in situ or used as an isolated compound without significant change in the reaction outcome.[40]

(39) Oxazolium-type salts **1b** and **5b** were found to be moisture sensitive and **2b** was very hygroscopic, thus precluding satisfactory elemental analysis.

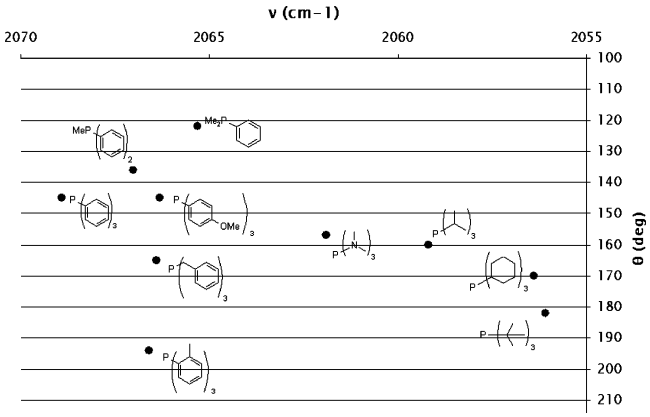

Figure 3. Tolman map of tested monoligating phosphines.

Ancillary Ligand Influence. Having established the breadth of the reaction, the role of the spectator ligand in a benchmark reaction was investigated. The reaction chosen was the coupling of 1-propyl-3-methylimidazolium bromide ([pmim]Br) with ethylene, in the presence of an in situ catalyst formed by mixing $Ni(COD)_2$ and an appropriate ligand.

The ligands employed in the reaction may be interpreted in terms of the "Tolman map"[41−43] plotted in Figure 3. While NHCs cannot be represented on a Tolman map because the cone angle (θ) model is unsuitable for characterization of their steric properties, work by Nolan and Cavallo introduced the buried sphere volume (% V_{Bur}) concept and these authors were able to conclude that, in terms of steric bulk, IMes is comparable with PCy_3, while IPr is closer to P^tBu_3.[44,45]

The phosphines employed in the study encompass a wide range of electronic and steric properties, with PPh_3 and P^tBu_3 lying at each extreme of the basicity scale and P(*o*-tolyl)$_3$ and Me_2PPh occupying the positions of most and least bulky ligands, respectively. Comparisons between PPh_3 and P(*p*-$OMeC_6H_4$)$_3$ on one hand and between P(*p*-$OMeC_6H_4$)$_3$ and P(CH_2Ph)$_3$ on the other provide an insight into the effect of independently varying ligand basicity and steric bulk, ν and θ. These are interesting and important comparisons, as will be seen later.

Table 3 shows the results obtained for the catalytic 2-substitution of imidazolium salts employing a range of different ligands sorted from least to most bulky (except for dppb, which cannot be compared to monodentate ligands). The catalytic reaction generally proceeds best with 2.1 equiv of ligand with respect to Ni (compare entries 3 and 4, 6 and 7, and 12 and 13), with the notable exception of the very bulky IPr, where excess ligand inhibits the reaction (Table 3; entries 18 and 19). In most cases, addition of further phosphine led to some reduction in performance, although decomposition of the catalyst could be suppressed by so doing.

Several of the more efficient catalyst systems were further tested using a low catalyst loading (1 mol %) and found to give good conversions (Table 3, entries 20−30). It was evident that the choice of solvent was also an important variable in this reaction.

(40) This adduct was found to be air sensitive and degraded to NH-benzothiazolium tetrafluoroborate when we tried to grow crystals for X-ray diffraction in order to elucidate its exact structure.

(41) Tolman, C. A. *J. Am. Chem. Soc.* **1970**, *92*, 2953−2956.
(42) Tolman, C. A. *J. Am. Chem. Soc.* **1970**, *92*, 2956−2965.
(43) Tolman, C. A. *Chem. Rev.* **1977**, *77*, 313−348.
(44) Hillier, A. C.; Sommer, W. J.; Yong, B. S.; Petersen, J. L.; Cavallo, L.; Nolan, S. P. *Organometallics* **2003**, *22*, 4322−4326.
(45) Dorta, R.; Stevens, E. D.; Scott, N. M.; Costabile, C.; Cavallo, L.; Hoff, C. D.; Nolan, S. P. *J. Am. Chem. Soc.* **2005**, *127*, 2485−2495.

Table 3. Selected Results with $Ni(COD)_2$[a]

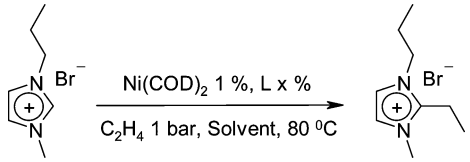

entry	solvent	ligand (mol %)	Conv (%)
1	DMF	dppb (11)	11
2	DMF	Me_2PhP (21)	95
3	DMF	$MePh_2P$ (11)	43[b]
4	DMF	$MePh_2P$ (21)	94
5	DMF	$MePh_2P$ (31)	81
6	DMF	PPh_3 (11)	<5[b]
7	DMF	PPh_3 (21)	24
8	DMF	$P(p\text{-}OMeC_6H_4)_3$ (21)	39
9	DMF	$P(NMe_2)_3$ (21)	<5[b]
10	DMF	$P(^iPr_3)$ (21)	88
11	DMF	$P(Bz)_3$ (21)	45
12	DMF	PCy_3 (11)	87
13	DMF	PCy_3 (21)	94
14	DMF	$P(^tBu)_3$ (21)	>95
15	DMF	$P(o\text{-tolyl})_3$ (21)	<5[b]
16	DMF	IMes (11)	94
17	DMF	IMes (21)	>95
18	DMF	IPr (21)	8
19	DMF	IPr (11)	93
20	DMF	PCy_3 (2.1)	<5
21	DMF	PCy_3 (1.1)	<5
22	DMF	$P(^tBu)_3$ (2.1)	<5
23	DMF	IMes (1.1)	<5
24	DMF	IPr (1.1)	<5
25	DMF	Me_2PhP (2.1)	26
26	DMA	Me_2PhP (2.1)	<5
27	DMSO	Me_2PhP (2.1)	<5
28	NMP	Me_2PhP (2.1)	83
29	THF/NMP (1/3)	Me_2PhP (2.1)	62
30	THF/NMP (2/1)	Me_2PhP (2.1)	52

[a] Reagents and conditions: 1-propyl-3-methylimidazolium bromide, 0.73 mmol; $Ni(COD)_2$, 10 mol % (entries 1−19), 1 mol % (entries 20−30); DMF, 3 mL; C_2H_4, 1 bar; 82 °C; 5 h; generally based on the average of two runs. [b] Rapid catalyst decomposition was observed.

Theoretical Study

In this section the coupling reaction of 1,3-dimethylimidazolium and ethylene was studied computationally to shed light on the experimental results.

As mentioned earlier, we envisaged a mechanism involving four main steps (Figure 2). This resulted in a full reaction sequence, as depicted in Figure 4: oxidative addition of the imidazolium salt (**1** → **4**), coordination of ethylene (**4** → **6b**), insertion of ethylene into the metal−hydride bond (**6b** → **9**), and reductive elimination of the coupled product (**9** → products).

Below we explore this mechanism using a range of ligand sets with varying degrees of bulk and basicity to reflect the catalysts employed in our experiments. The ligand sets used include the following: $L_1 = L_2$ = 1,3-dimethylimidazol-2-ylidene (dmiy); L_1 = dmiy, L_2 = trimethylphosphine (PMe_3); $L_1 = L_2 = PMe_3$; $L_1 = L_2$ = triphenylphosphine (PPh_3); $L_1 = L_2$ = tri-*tert*-butylphosphine (P^tBu_3).

Starting Complexes (1). In general, the calculated starting complexes were optimized as expected. The $Ni(dmiy)_2$ calculated geometry is in excellent agreement with known crystal structures of similar complexes[11,46] (Table 4), with a calculated nickel−carbene bond distance of 1.825 Å and a near-linear arrangement of the ligands. In contrast, the nickel−phosphine starting complexes display a slightly bent configuration, allowing an "open" side for solvation or substrate coordination. The sole exception is the extremely bulky $Ni(P^tBu_3)_2$, which was optimized in a linear configuration.

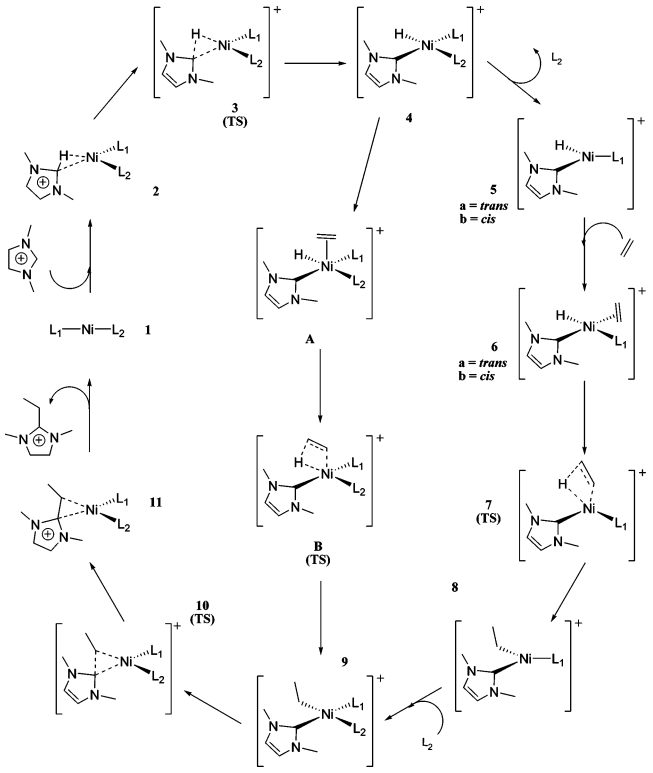

Figure 4. Full catalytic cycle for coupling of ethylene and imidazolium salts.

Table 4. NiL_1L_2 Starting Complex Bond Distances and Angles

NiL_1L_2	Ni−L_1 (Å)	Ni−L_2 (Å)	L_1−Ni−L_2 (deg)
$L_1 = L_2$ = IMes[a]	1.827	1.830	177.4
$L_1 = L_2 = I^tBu$[b]	1.874	1.874	180
$L_1 = L_2$ = dmiy[c]	1.823	1.823	164.5
L_1 = dmiy; $L_2 = PMe_3$[c]	1.805	2.064	137.7
$L_1 = L_2 = PMe_3$[c]	2.059	2.059	129.5
$L_1 = L_2 = PPh_3$[c]	2.094	2.092	155.7
$L_1 = L_2 = P^tBu_3$[c]	2.135	2.136	178.7

[a] Crystal structure (IMes = dimesitylimidazol-2-ylidene).[46] [b] Crystal structure (ItBu = di-*tert*-butylimidazol-2-ylidene).[11] [c] Calculated.

The Ni(dmiy)(PMe_3) Ni−L bond distance reflects the σ-donor strength of the carbene ligands compared to that of their phosphine counterparts, with an extended nickel−phosphine distance of 2.064 Å and reduced nickel−carbene distance of 1.805 Å.

Oxidative Addition (1 to 4). Theoretical studies indicate that the oxidative addition of imidazolium salts to group 10 metals initially occurs via an interaction between the metal center and C2 of the salt,[5,6,15,17,18,25] leading to a concerted three-centered transition structure, in which the C2−H bond elongates as the salt draws closer to the metal.

In this work, no precursor complex or transition structure was found for the larger $Ni(PPh_3)_2$ and $Ni(P^tBu_3)_2$ systems. While a small reaction barrier may exist, introduction of the imidazolium salt into the reaction sphere of the metal resulted directly in the oxidative addition product, with no stable encounter complex as found for the smaller ligand systems.

The product in the majority of cases was the four-coordinate square-planar nickel(II) hydride complex **4**, where, once again,

(46) Anthony J.; Arduengo, I.; Gamper, S. F.; Calabrese, J. C.; Davidson, F. *J. Am. Chem. Soc.* **1994**, *116*, 4391−4394.

Table 5. Ni(NHC)(H)L_1L_2 Bond Distances[a]

system	Ni−NHC	Ni−H	Ni−L_1	Ni−L_2
$L_1 = L_2 =$ IMes[b]	1.891	1.38	1.895	1.936
$L_1 = L_2 =$ dmiy[c]	1.895	1.482	1.895	1.923
$L_1 =$ dmiy; $L_2 = PMe_3$[c]	1.884	1.478	1.893	2.206
$L_1 = L_2 = PMe_3$[c]	1.881	1.475	2.193	2.208
$L_1 = L_2 = PPh_3$[c]	1.863	1.453	2.238	2.232
$L_1 = P^tBu_3$[c,d]	1.841	1.408	2.242	

[a] Legend: L_1, trans dmiy; L_2, trans H. [b] Crystal structure (L_1= dimesitylimidazol-2-ylidene (IMes); L_2 = 1-butyl-3-methylimidazol-2-ylidene).[17] [c] Calculated. [d] Three-coordinate structure.

calculated structures for the $NiH(dmiy)_3$ complex agreed favorably with known crystal structures (Table 5).

The increasing basicity of the trans ligand led to an increase in the associated metal−hydride bond length (Table 5). The exception was the $Ni(P^tBu_3)_2$ system, where the bulk of the ancillary ligands caused excessive congestion around the reacting metal center and, consequently, dissociation of a phosphine ligand was required before interaction of the imidazolium salt could occur. As a result a more compact three-coordinate structure was observed for the $Ni(P^tBu_3)_2$ system.

The oxidative addition step was found to be very exothermic in all systems with early transition structures, and as a result, minimal activation energies were observed (Figure 5). While solvation may somewhat stabilize the Ni(0) starting complexes, calculations indicate the initial oxidative addition step appears to be a facile entry point to the catalytic cycle for all systems.

Ethylene Coordination (4 to 6b). For the catalytic cycle to continue after the oxidative addition step, the alkene must be able to coordinate in the appropriate mode to the metal center before subsequent insertion into the metal−hydride bond. Coordination and insertion may occur in different ways, as shown in Figure 6: a dissociative route (route a) and an associative route involving a five-coordinate metal center (route b) were envisaged.[47]

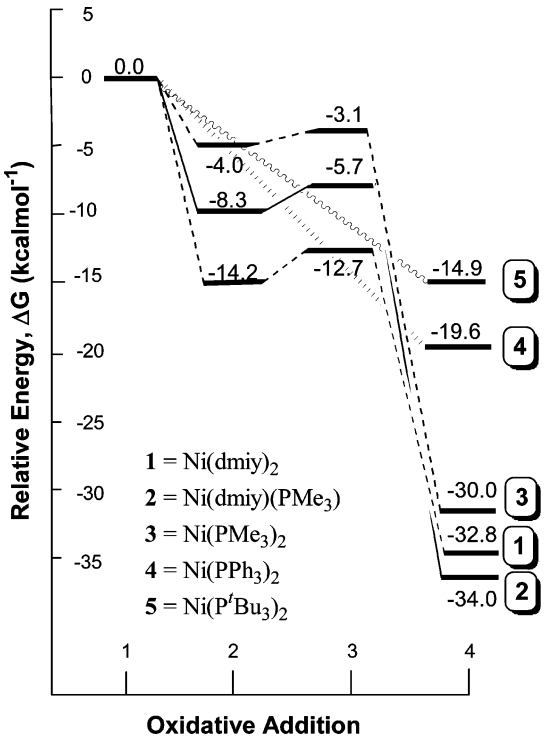

Figure 5. Energies for the oxidative addition step (three-coordinate structure for P^tBu_3).

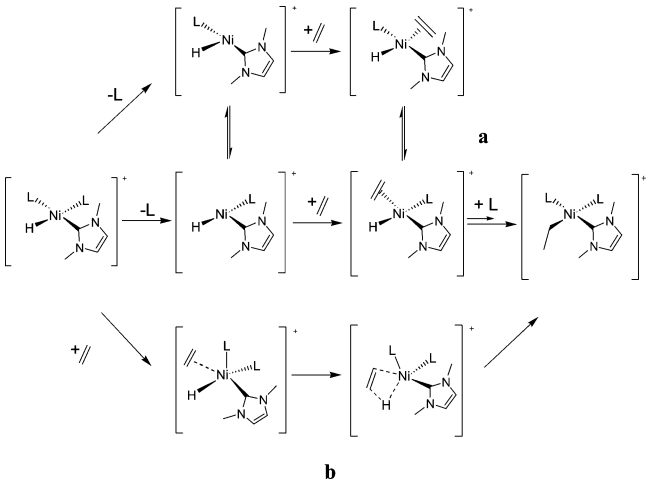

Figure 6. Possible ethylene coordination mechanisms: (a) dissociative route; (b) associative route.

For the associative route, only the smaller $Ni(dmiy)_2$, $Ni(PMe_3)_2$, and $Ni(dmiy)(PMe_3)$ systems afford enough room in the metal coordination sphere for five ligands. Despite the detection of this associative route for the smaller ligands, the energy required for ethylene insertion was found to be much higher than the corresponding dissociative routes, with activation energies of 42.1, 42.4, and 30.8 kcal mol^{-1} from the Ni(H)-$(dmiy)L_1L_2$ oxidative addition product for $Ni(dmiy)_2$, Ni(dmiy)-(PMe_3), and $Ni(PMe_3)_2$, respectively. As relatively low energy three-coordinate structures were located, it is likely that this is the preferred route, with ethylene coordination occurring after dissociation of an ancillary ligand from the $Ni(H)(dmiy)L_1L_2$ complex (**4**).

Dissociation of a carbene ligand in the $Ni(dmiy)_2$ system is very unfavorable, with 27.1 and 38.5 kcal mol^{-1} activation energies for ligands trans and cis to the hydride ligand, respectively (Figure 7). dmiy is a very compact ligand, and NHCs form very strong metal bonds: two factors that mitigate against ligand dissociation. Despite the difficulty envisaged for the dissociation of the dmiy ligand, it has been revealed experimentally that NHCs can be excellent in promoting the overall catalytic process. While this may appear contradictory to the calculations herein, the two NHC ligands successfully employed experimentally (i.e. IMes and IPr) are much bulkier species and may behave more like PCy_3 or P^tBu_3, as described below.

Phosphine dissociation for the PMe_3 ligand also appears relatively challenging, requiring 20.6 and 30.2 kcal mol^{-1} for dissociation of the ligand trans and cis to the hydride, respectively. This reduces slightly to 17.1 kcal mol^{-1} (trans) and 28.5 kcal mol^{-1} (cis) for the mixed carbene/phosphine system. As expected, using the larger and more weakly bound PPh_3 reduces the dissociation activation energies considerably, requiring 9.2 and 12.0 kcal mol^{-1} for formation of the three-coordinate trans and cis intermediates, respectively. Finally, for the P^tBu_3 system, oxidative addition proceeds through a dissociative route; therefore, subsequent ethylene coordination occurs directly from the oxidative addition product with no further dissociation required.

In all cases, dissociation of the ligand trans to the hydride (**5a**) was more facile than the related cis dissociation (**5b**) (Figure 7). This would imply that ethylene coordination would occur in the trans position and, consequently, isomerization

(47) Shultz, C. S.; DeSimone, J.; Brookhart, M. *Organometallics* **2001**, *20*, 16−18.

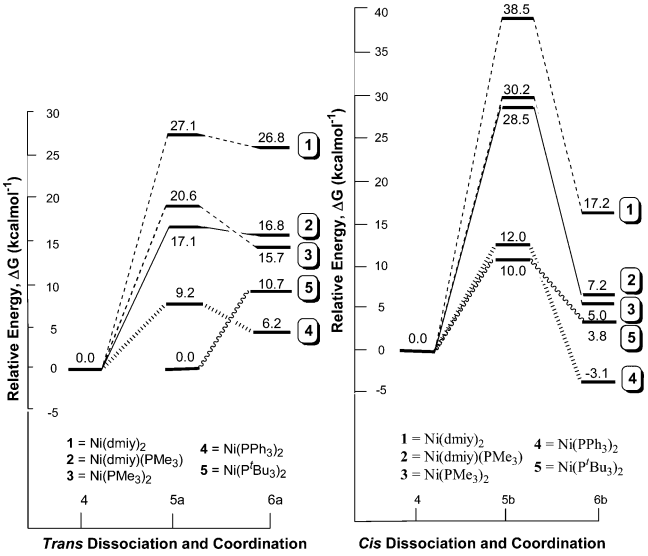

Figure 7. Ethylene coordination step via cis and trans dissociation.

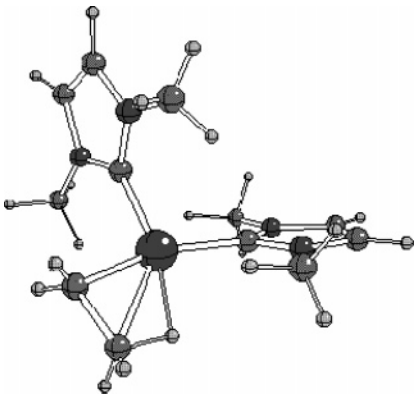

Figure 8. Example of a nickel hydride ethylene cis complex.

would be required for continuation of the cycle, as a cis geometry is required for ethylene insertion. Whether this occurs before or after ethylene coordination via an inter- or intramolecular rearrangement or a solvent-mediated rearrangement was not investigated. However, once coordinated, the cis forms of the NiH(dmiy)L(ethylene) complexes (**6b**) are significantly more stable than the associated trans forms (**6a**).

Ethylene Insertion (6b to 9). On formation of the cis form of the ethylene complex, insertion of the ethylene into the metal−hydride bond is relatively facile. Examination of the cis-coordinated complexes (**6b**) reveals an interesting geometry in which there is a stable interaction between the hydride ligand and the adjacent ethylene (Figure 8). In all cases, this interaction is significantly more stable than the more traditional four-coordinate square-planar complex, in which the ethylene ligand is perpendicular to the plane of the metal and the remaining ligands.

Insertion of the ethylene ligand into the metal−hydride bond becomes straightforward from the ethylene hydride cis complex (Figure 9). The smaller ligands only require around 10 kcal mol^{-1} to twist the ethylene to form the insertion transition structure **7**, with recoordination of the expelled ligand to form a four-coordinate complex, further stabilizing the product **8**.

While the larger PPh_3 system also only require 10.4 kcal mol^{-1} for ethylene insertion, recoordination of the free PPh_3 ligand results in the less stable four-coordinate product **9**, due to crowding of the metal center. Similarly, the P^tBu_3 system

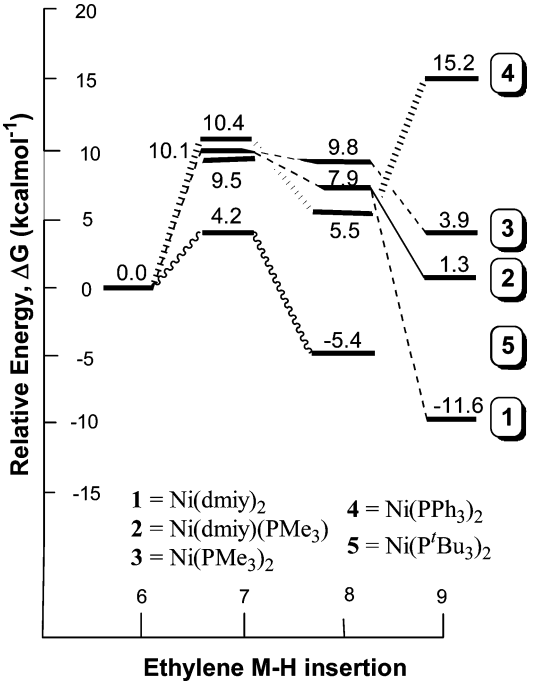

Figure 9. Energies for the ethylene insertion step.

disfavors recoordination of the ligand, with the product significantly favoring the three-coordinate ethyl complex.

Overall, calculations indicate that once the correct cis form of the complex has formed, ethylene rearrangement and insertion are facile for all systems. In particular, P^tBu_3 displays a significantly reduced barrier to insertion and a correspondingly stable product. However, it must be remembered that, in this case, the initial four-coordinate ethylene hydride complex **6b** is relatively high in energy.

Reductive Elimination (9 to Products). The reductive elimination step previously identified for other group 10 metal carbene complexes was mirrored in the catalytic cycle studied here.[4−7] A concerted three-center transition structure was formed in which a carbene ligand and a cis-located ethyl group approach each other and later draw away from the metal center to create the 2-ethylimidazolium salt and re-form the original nickel(0) complex.

For the four-coordinate complexes, the activation energy to reductive elimination was found to range from 18.6 kcal mol^{-1}, in the case of PPh_3, to 23.3 kcal mol^{-1} for dmiy (Figure 10). This can be rationalized by taking into account both steric and electronic effects: basic and/or compact ligands are expected to be more reluctant to undergo reductive elimination. PPh_3 is the bulkiest and least basic of the three ligands (dmiy, PMe_3, and PPh_3); therefore, it is not surprising that it should be the ligand that most effectively promotes reductive elimination, while dmiy is the most basic and most compact ligand and thus displays the highest activation energy. Other complexes fall perfectly between these extremes.

As mentioned in the previous section, recoordination of a PPh_3 ligand to form the four-coordinate ethyl complex **9** is an endothermic process. Therefore, we examined the possibility of reductive elimination from the three-coordinate ethyl complex **8**. With only one phosphine attached directly to the metal center, the remaining ligands display shorter bond lengths to the metal than do their four-coordinate counterparts, and the more compact nature of the three-coordinate complex makes it more susceptible to reductive elimination with an activation energy of only 16.6

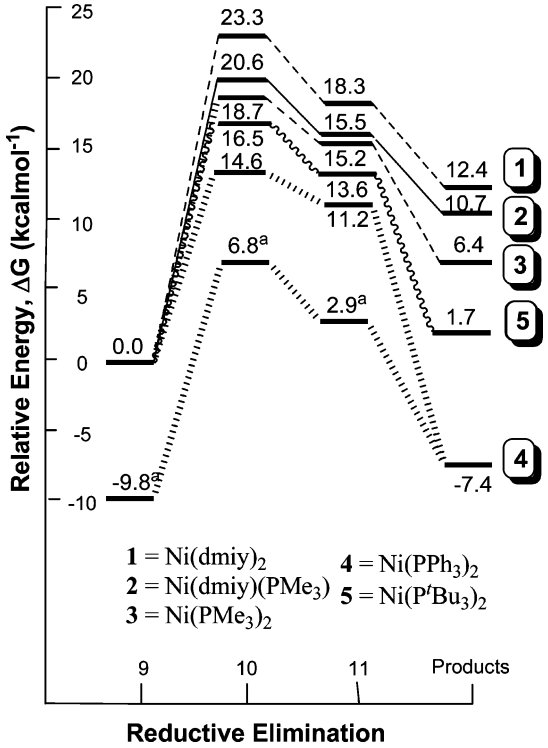

Figure 10. Energies for the reductive elimination step. The superscript "a" indicates the monophosphine route.

kcal mol^{-1} (Figure 10). Similarly, the Ni(P^tBu_3)$_2$ system has a low reductive elimination activation energy of 16.5 kcal mol^{-1}.

An interesting consequence of the endothermic reductive elimination step is the impact on the reverse reaction (i.e., oxidative addition of 2-ethyl-1,3-dimethylimidazolium to afford the four-coordinate ethyl complex **9**). In all cases, this reverse reaction is favored both kinetically (lower activation energy) and thermodynamically (more stable product), indicating that "blocking" the C2 position of imidazolium salts with an alkyl group[6,48,49] might not be effective against oxidative addition with particularly reactive complexes. That being said, reversal of this step during this catalytic reaction is unlikely, as continuation of the cycle by replacement of the loosely bound 2-ethylimidazolium by a new 1,3-dimethylimidazolium salt presents a lower barrier to reaction than does the reverse oxidative addition of the 2-ethylimidazolium.

Overall, as an individual step the reductive elimination introduces a considerable barrier for all catalytic systems. The least demanding route is the highly compact Ni(P^tBu_3)$_2$ system with a relatively high energy ethyl complex (**8**) and a lower energy transition structure (**10**).

Summary of Theoretical Data. Two important parameters for catalysis are the energy difference, or energetic span (δE), between the most abundant reaction intermediate (MARI) and the highest energy transition state (HETS)[50] and the maximum activation energy (ΔE_{max}) between two consecutive intermediates. An efficient process should have the smallest possible value for δE, as under steady-state conditions the rate of the reaction is limited by this parameter and the most general way of improving a catalytic process (apart from preventing catalyst decomposition) consists of stabilizing the HETS and/or destabilizing the MARI.[20,21,51] On the other hand, ΔE_{max} often determines the so-called "rate determining step" (rds) of the reaction. If an rds exists (i.e., if all the other activation energies can be neglected,[52] improvement of the reaction kinetics can only be achieved by reducing the energy of this step. If the maximum activation energy cannot be easily overcome and causes the catalyst to be "stored" along the reaction pathway, steady-state conditions may not be reached and catalysis (in the true sense) becomes impossible, with only a few turnover numbers (TON) being achieved as a result. These considerations are important, because they underline the differences between true catalytic conditions (i.e., steady-state conditions, high TONs) and "pseudo-catalytic" or substoichiometric conditions (more complex kinetics, low TONs). Calculated results for the δE and ΔE values are shown in Table 6.

Table 6. δE and ΔE_{max} Parameters

system	MARI[a]	HETS[a,b]	δE[a]	ΔE_{max}[a] (step)
$L_1 = L_2 =$ dmiy	−32.8	5.7	38.5	38.5 (D[c])
$L_1 =$ dmiy, $L_2 = PMe_3$	−34.0	−4.9	29.1	28.5 (D)
$L_1 = L_2 = PMe_3$	−30.0	0.2	30.2	30.2 (D)
$L_1 = L_2 = PPh_3$ (assoc)	−22.7	7.1	29.8	24.3 (RE[d])
$L_1 = L_2 = PPh_3$ (dissoc)	−22.7	−0.6	22.1	16.6 (RE)
$L_1 = L_2 = P^tBu_3$	−16.5	0.0	16.5	16.5 (RE)

[a] In kcal mol^{-1}. [b] Excluding separated reactants. [c] Ligand dissociation from NiH(dmiy)L_2. [d] Reductive elimination.

Several conclusions may be drawn from this computational study. First, the oxidative addition step affording a nickel hydride is exothermic for widely different ligands, from the compact and extremely basic dmiy to the bulkier and less basic PPh_3. Consequently, this step is not expected to be rate determining under experimental conditions.

Second, our calculations reveal a very interesting behavior for P^tBu_3. Its steric bulk appears to favor the formation of a monophosphine nickel complex during the whole cycle, making the coordination sphere much more compact (short metal to ligand distances) and, thus, sterically encumbered. This has two main effects—to make olefin coordination more difficult and, importantly, reductive elimination facile. This more compact nature of monophosphine complexes magnifies the importance of the steric bulk of the phosphine ligand in reductive elimination, which is the last step in many C−C bond forming processes. So-called monoligated complexes of Pd have recently been the focus of experimental and computational investigations.[53−55]

Third, it appears that a "monophosphine route" favoring three-coordinate intermediates is similarly plausible for PPh_3. When the values of the δE and ΔE parameters were initially compared, it was apparent that the associative PPh_3 system displayed a high δE at 29.8 kcal mol^{-1}. As this system is active under relatively mild conditions,[19] the high δE value suggests that the alternative dissociative pathway might be active. With an δE value of 22.1 kcal mol^{-1}, this route is highly probable and it is likely that both the oxidative addition and reductive elimination steps would go via a monophosphine complex under experimental conditions.

From these results, the NiL_1L_2 catalytic systems appear to fall into three separate categories.

(48) Chianese, A. R.; Kovacevic, A.; Zeglis, B. M.; Faller, J. W.; Crabtree, R. H. *Organometallics* **2004**, *23*, 2461−2468.
(49) Chianese, A. R.; Zeglis, B. M.; Crabtree, R. H. *Chem. Commun.* **2004**, 2176−2177.
(50) Kozuch, S.; Shaik, S. *J. Am. Chem. Soc.* **2006**, *128*, 3355−3365.
(51) Kozuch, S.; Amatore, C.; Jutand, A.; Shaik, S. *Organometallics* **2005**, *24*, 2319−2330.
(52) Campbell, C. T. *J. Catal.* **2004**, *204*, 520−524.
(53) Christmann, U.; Vilar, R. *Angew. Chem., Int. Ed.* **2005**, *44*, 366−374.
(54) Ahlquist, M.; Fristrup, P.; Tanner, D.; Norrby, P.-O. *Organometallics* **2006**, *25*, 2066−2073.
(55) Ahlquist, M.; Norrby, P.-O. *Organometallics* **2007**, *26*, 550−553.

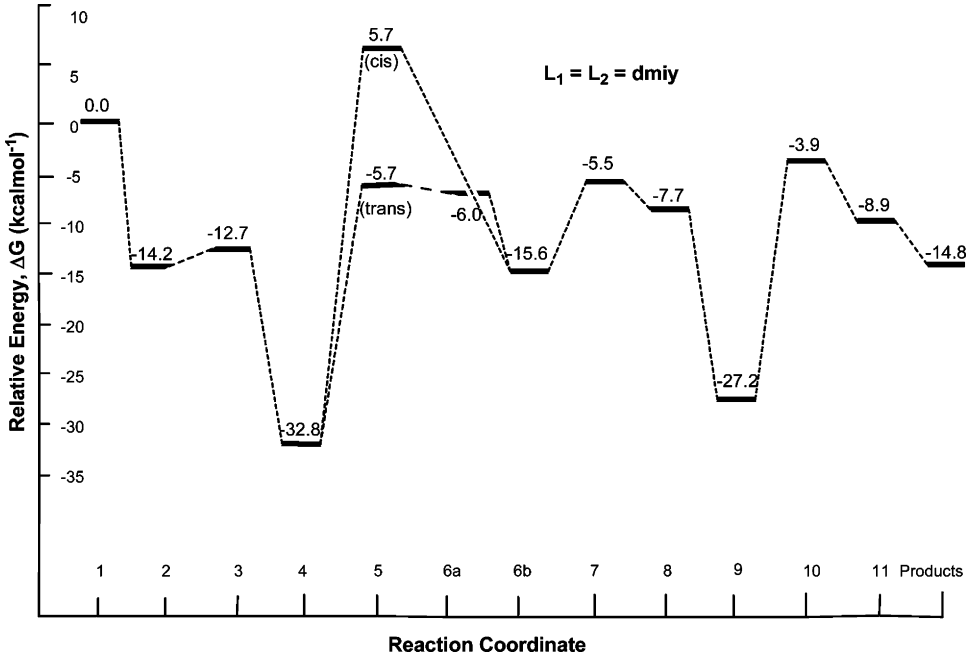

Figure 11. Full energy diagram for the Ni(dmiy)$_2$ system.

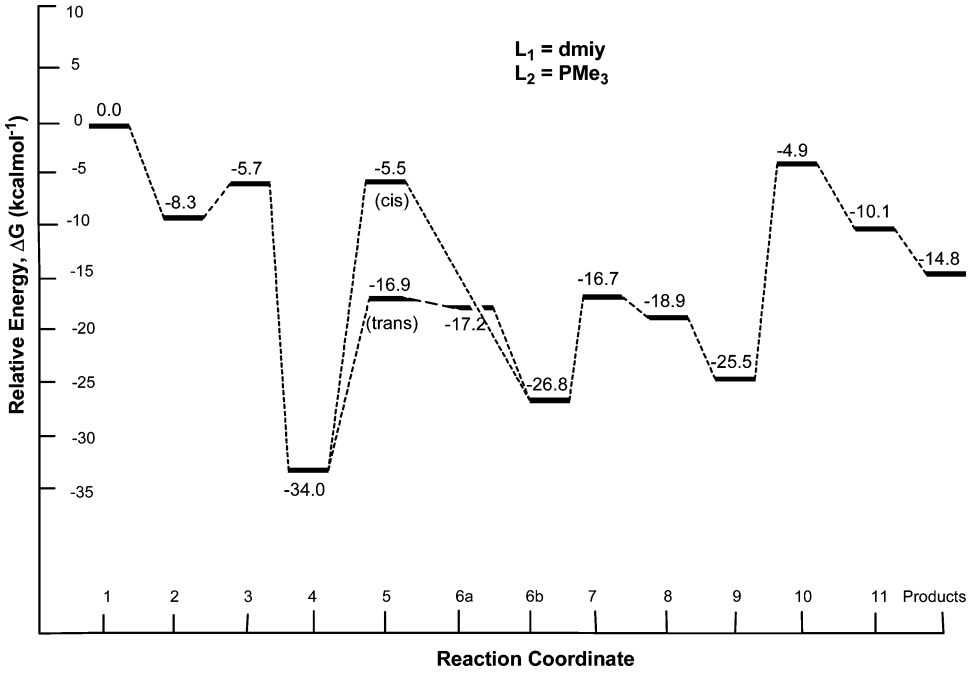

Figure 12. Full energy diagram for the Ni(dmiy)(PMe$_3$) system.

Case 1: for the smallest, less easily dissociated ligands such as dmiy and PMe$_3$, four-coordinate complexes would be favored and as a result the main activation energy becomes ligand dissociation prior to ethylene coordination (Figures 11−13).

Case 2: for larger, labile phosphines, ethylene is more easily coordinated and reductive elimination becomes the rate-determining step. Calculations indicate two possible routes, with one or two phosphine ligands on Ni (Figure 14).

Case 3: for very bulky, more readily dissociated ligands (e.g., P^{t}Bu$_3$), catalysis proceeds via more compact monophosphine intermediates in which ethylene coordination is challenging, but reductive elimination remains the rate-determining step (Figure 15).

Comparison of Experiment and Theory. There is, in general, excellent agreement between the experimental observations and the theoretical results. Initially it was difficult to interpret the experimental results; however, when they are taken in conjunction with the computational studies, it becomes apparent that the reaction is a complex and "flexible" process, in which different rate-determining steps operate, depending on the ancillary ligand employed.

Steric bulk appears to be the predominant factor affecting the rate-determining step. Just where the reaction changes from a mono- to diphosphine system is unclear, but experiments seem to indicate that it could be where cone angles are around 160°. With this in mind, experimental results can also be divided into three classes. As observed from the computational studies, case 1 represents phosphine cone angles of less than 140°, case 2 operates for cone angles between 140° and around 160°, and case 3 is in operation when cone angles exceed 160° (Table 7).

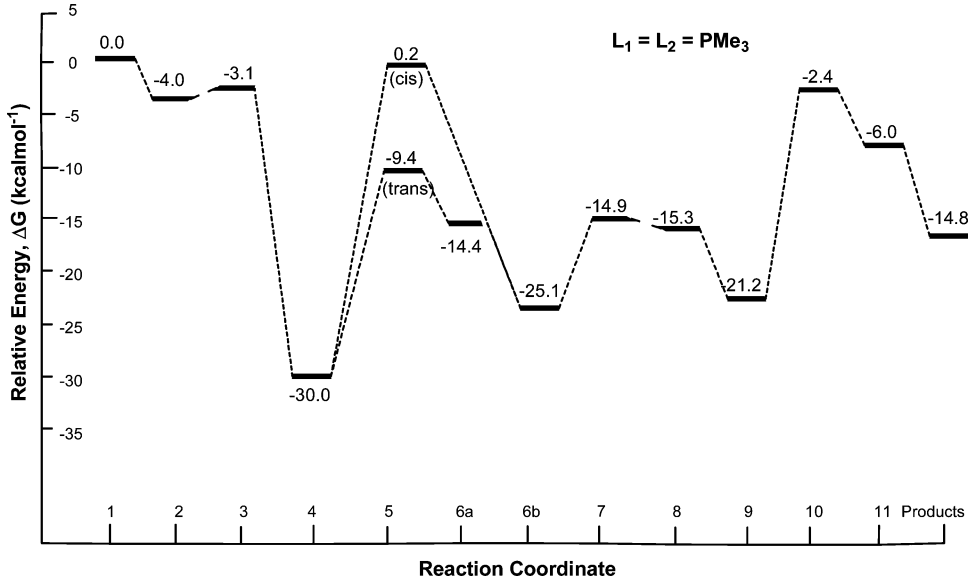

Figure 13. Full energy diagram for the $Ni(PMe_3)_2$ system.

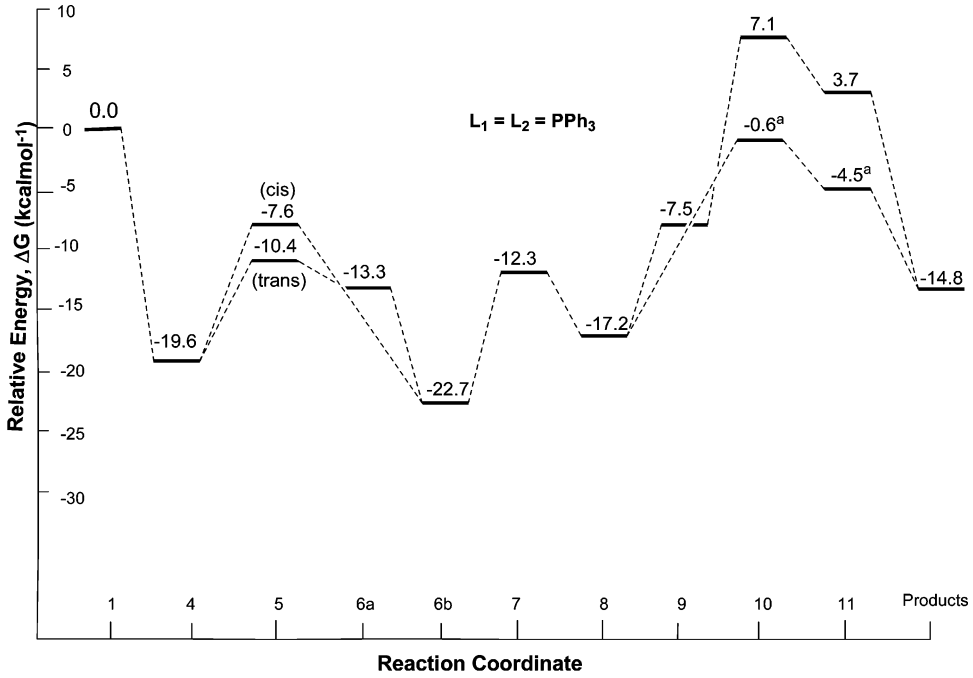

Figure 14. Full energy diagram for the $Ni(PPh_3)_2$ system. The superscript "a" indicates monophosphine reductive elimination.

Consistent with the theoretical studies, it was noted that smaller and more basic phosphines, such as PMe_2Ph and $PMePh_2$, accommodate 2 equiv of ligand and any excess phosphine (more than 2 equiv) retards the reaction by competing with incoming substrate. For example, take the case of $PMePh_2$ (Table 7, case 1): 1.1 equiv of ligand catalyzed the reaction, albeit with significant catalyst decomposition, while 2.1 equiv gave the best results. A significant decrease in activity was observed when 3.1 equiv of ligand was used, which is consistent with ligand dissociation being the rds.

In terms of steric influence, calculations found PPh_3 to be a borderline case, with both associative and dissociative mechanisms possibly operating and reductive elimination being the rds (case 2). Replacing PPh_3 by $P(p\text{-}OMeC_6H_4)_3$ (i.e., increasing basicity but leaving bulk unchanged; Table 7, case 2), generates an increase in yield. This result is attributed to reduced catalyst decomposition, with the more basic ligand stabilizing the Ni intermediates.

For larger phosphine ligands, a dissociative mechanism is expected to operate uniformly. Here, due to steric constraints, ethylene coordination is challenging; however, reductive elimination remains the rate-determining step (case 3). In the cases of PCy_3 ($\theta = 170°$) and P^tBu_3 ($\theta = 182°$), a small excess of ligand was beneficial; no nickel black was observed with 2.1 equiv (Table 3, entries 12−14). For these systems, a small amount of additional ligand may simply improve catalyst stability without significantly affecting the ligand dissociation equilibrium.

As mentioned previously, IMes may be considered similar in bulk to PCy_3 and IPr similar to P^tBu_3, which most closely links them to case 3. Interestingly, only the IMes system demonstrated good activity when 2.1 equiv of ligand was used (Table 3, entry 17). Using proportions of 1.1 equiv, both ligand systems demonstrated very high activities (Table 3, entries 16 and 19). The extremely bulky nature of IPr and the intrinsically strong coordinating ability of carbenes probably explain this

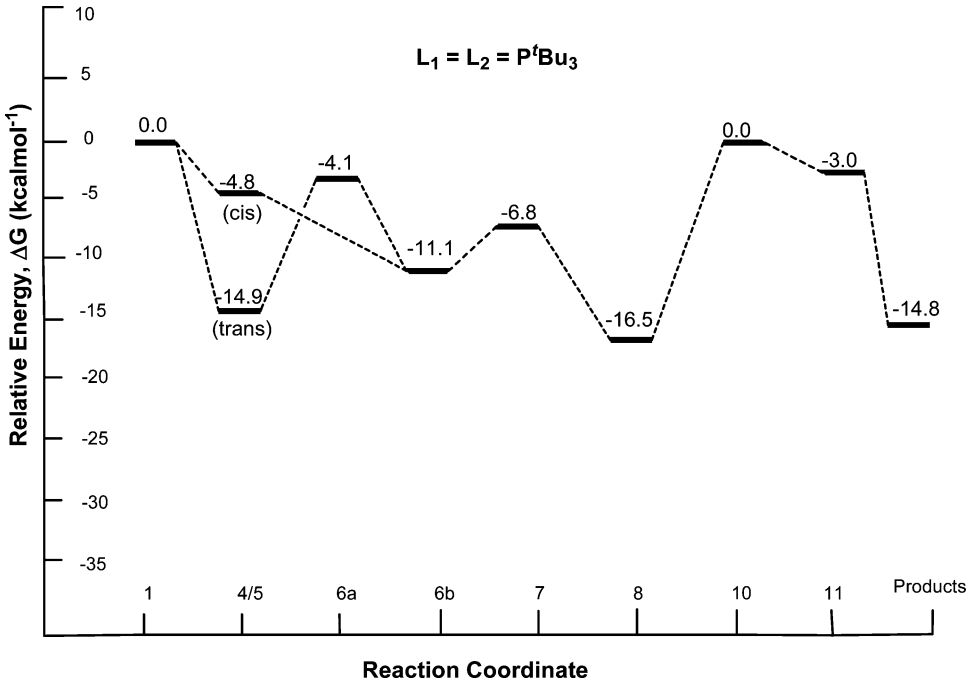

Figure 15. Full energy diagram for the $Ni(P^tBu_3)_2$ system.

Table 7. Experimental Results Grouped in Three Cases[a]

case	ligand (mol %)	Conv (%)
1	Me_2PhP (21)	95
1	$MePh_2P$ (11)	43
1	$MePh_2P$ (21)	94
1	$MePh_2P$ (31)	81
2	PPh_3 (21)	24
2	$P(p\text{-}OMeC_6H_4)_3$ (21)	39
3	$P(^iPr_3)$ (21)	88
3	$P(Bz)_3$ (21)	45
3	PCy_3 (21)	94
3	$P(^tBu)_3$ (21)	>95
3	IMes (11) (~PCy_3)	94
3	IMes (21)	>95
3	IPr (21) (~P^tBu_3)	8
3	IPr (11)	93

[a] See Table 3 for reaction conditions.

observation. Although IPr is comparable to P^tBu_3 in terms of steric bulk, it is a much stronger σ donor and $Ni(IPr)_2$ can be synthesized from $Ni(COD)_2$ and free IPr,[56] whereas (to the best of our knowledge) $Ni(P^tBu_3)_2$ has not been isolated (in this case the complex formation equilibrium strongly favors phosphine dissociation).[57] Therefore, it is likely that, under our conditions, the sterically crowded but stable $Ni(IPr)_2$ forms and is unable to enter the catalytic cycle. In contrast, activity is retained in the case of the less sterically demanding IMes (entries 16 and 17).[58]

Finally, a hemilabile chelating phosphine, namely dppb (bis-(diphenylphosphino)butane) gave poor results, most probably because of considerably slower and/or thermodynamically disfavored reductive elimination from a chelate complex.[7] This would confirm that chelation is an effective way of stabilizing hydrocarbyl complexes of NHCs under catalytic conditions.[4]

(56) Louie, J.; Gibby, J. E.; Farnworth, M. V.; Tekavec, T. N. *J. Am. Chem. Soc.* **2002**, *124*, 15188−15189.

(57) Ogoshi, S.; Ueta, M.; Oka, M.-A.; Kurosawa, H. *Chem. Commun.* **2004**, 2732−2733.

(58) Campeau, L.-C.; Thansandote, P.; Fagnou, K. *Org. Lett.* **2005**, *7*, 1857−1860.

General Conclusions

The combined experimental and DFT study of the reaction of ethylene with imidazolium salts has provided valuable insight into this process. The catalytic reaction we have described is relatively complex, with a number of possible rate-determining steps apparent, each of which can become dominant when ligands are changed. The trends in catalytic behavior can now be understood with some confidence: systems incorporating smaller ligands such as PMe_3 and dmiy are better described by an associative route, in which ligand dissociation is the rate-determining step. This was confirmed experimentally in the case of $PMePh_2$. Larger ligands such as PPh_3 and P^tBu_3 are expected to react via a "monophosphine" route, in which the rate-determining step would be reductive elimination. Bulky ligands that are also strongly electron donating gave higher activity, probably due to stabilization of the catalyst. The two NHC ligands tested (IMes and IPr) also seem to belong to this category, indicating that care must be taken using simple carbenes such as dmiy to model their behavior.

Experimental Section

General Comments. All manipulations were carried out using standard Schlenk techniques under an Ar or N_2 atmosphere or using an MBraun M72 glovebox (N_2 atmosphere with <1 ppm of O_2 and H_2O), where all chemicals were stored. THF and toluene were dried and freshly distilled before use (sodium benzophenone ketyl and sodium metal, respectively). Acetone was dried and distilled over B_2O_3 and stored under an inert atmosphere. Anhydrous DMF and NMP were purchased from Aldrich and transferred under Ar in a Young Schlenk flask containing activated 4 Å molecular sieves. Phosphine ligands were purchased from Strem. ^1H and ^{13}C NMR chemical shift values are reported relative to the residual solvent peak.

NHC ligands were synthesized using reported procedures.[59] $Ni(COD)_2$ was synthesized from $Ni(acac)_2$ according to a known

(59) Anthony J. Arduengo, I.; Krafczyk, R.; Schmutzler, R.; Craig, H. A.; Goerlich, J. R.; Marshall, W. J.; Unverzagt, M. *Tetrahedron* **1999**, *55*, 14523−14534.

procedure,[60] except that a larger excess of COD (3.5 equiv) was used instead of the much more hazardous 1,3-butadiene.

General Procedure for the Azolium−Alkene Coupling Reaction. A 60 mL Young Schlenk flask was charged with bis(cycloocta-1,5-diene)nickel(0) (0.073 mmol), triphenylphosphine (0.15 mmol), and the azolium salt (0.73 mmol) in a glovebox. Under a flow of ethylene, acetone (9 mL) and THF (3 mL) were then syringed into the reaction vessel and the orange-yellow solution was heated to 55 °C. The Schlenk vessel was then pressurized to 1 bar with ethylene and closed. The solution was stirred for 48 h, during which time variable amounts of Ni(0) black formed. The solvents were then removed in vacuo, and the residue was taken up into CD_2Cl_2 or d_6-DMSO and submitted for ^{1}H NMR. Conversions were estimated by relative integration of the product's ethyl CH_2 group and the starting material's C2 proton (low conversions) or NCH_3 group (high conversions).

Separation and isolation of the azolium coupling products was carried out according to the following procedure.

DCM or acetone (20 mL) was added to the crude reaction mixture. The mixture was stirred at room temperature for 15 min and then filtered through a pad of Celite. The solvent was concentrated under vacuum to a minimum, and a precipitate formed upon addition of hexane (10−15 mL). After the solvent was decanted off, the precipitate was further recrystallized from DCM/hexane or DCM/diethyl ether mixtures (one to three times) and finally dried under vacuum to afford the azolium coupling products with isolated yields within 5−15% of estimated values found by ^{1}H NMR.

The procedure for the catalytic functionalization of azolium salts was adapted for the ligand study: DMF (3 mL) was used as a solvent and injected under a flow of N_2. Then the solution was heated to 80 °C and bubbled for 1 min with ethylene and the vessel pressurized to 1 bar. The reaction mixture was stirred for 5 h at 80 °C. d_6-DMSO was used as NMR solvent.

Benzothiazole Functionalization. Benzothiazole−BF_3 (0.73 mmol) adduct[61] was placed in a Young Schlenk flask in the glovebox, together with $Ni(COD)_2$ (10 mol %) and the ligand (20 mol %). The same procedure as that used for the ligand study was then used, with either anhydrous BTF (purchased from Aldrich) or toluene. The reaction mixture was cooled down, the solvent was evaporated at room temperature, and the residue was partitioned with water/dichloromethane. The organic phase was dried over $MgSO_4$ and analyzed by GCMS. The identity of the product of the reaction was confirmed by a preparative-scale run, in which 2-ethylbenzothiazole was obtained after distillation and analyzed by ^{1}H NMR and GCMS.

3,4,5-Trimethylthiazolium Tetrafluoroborate (1a).[62] Trimethyloxonium tetrafluoroborate (600 mg, 4.1 mmol) was added in portions to a solution of 4,5-dimethylthiazole (482 mg, 4.3 mmol) in DCM (10 mL). The mixture was stirred at room temperature for 18 h before the volatiles were removed in vacuo and the residue was washed with diethyl ether (3 × 5 mL). Finally the product was dried in vacuo to afford a white solid (yield: 752 mg, 86%). ^{1}H NMR (d_6-DMSO, 400 MHz): δ 9.91 (s, 1H, C2H), 4.07 (s, 3H, NCH_3), 2.49/2.40 (2 × s, 2 × 3H, CCH_3). ^{13}C NMR (d_6-DMSO, 100.63 MHz): δ 155.5 (C2), 142.1/132.3 (C4,5), 40.1 (NCH_3), 11.7/10.8 (CCH_3).

3-Methylbenzothiazolium Tetrafluoroborate (2a).[63] This compound was prepared in the same manner as for **1a** from trimethyloxonium tetrafluoroborate (500 mg, 3.4 mmol) and benzothiazole (480 mg, 3.6 mmol) to give an off-white solid (yield: 665 mg, 83%). ^{1}H NMR (d_6-acetone, 400 MHz): δ 10.54 (s, 1H, C2H), 8.56 (d, 1H, $^3J_{HH}$ = 8.2 Hz, arom CH), 8.45 (d, 1H, $^3J_{HH}$ = 8.5 Hz, arom CH), 8.04 (m, 1H, arom CH), 7.95 (m, 1H, arom CH), 4.66 (s, 3H, NCH_3). ^{13}C NMR (d_6-DMSO, 100.63 MHz): δ 164.8 (C2), 141.0/131.1 (C8,9), 129.4/128.3/124.9/117.0 (arom CH), 39.3 (NCH_3).

3-Methyloxazolium Tetrafluoroborate (3a).[64] Trimethyloxonium tetrafluoroborate (600 mg, 4.1 mmol) was added in portions to a solution of oxazole (294 mg, 4.3 mmol) in acetone (10 mL). The mixture was stirred at 55 °C for 17 h before the volatiles were removed in vacuo and the residue washed with diethyl ether (3 × 5 mL). Finally the product was dried in vacuo to afford a white solid (yield: 423 mg, 61%). ^{1}H NMR (d_6-DMSO, 400 MHz): δ 10.17 (s, 1H, C2H), 8.74/8.22 (2 × s, 2 × 1H, C4,5), 3.93 (s, 3H, NCH_3). ^{13}C NMR (d_6-DMSO, 100.63 MHz): δ 155.4 (C2), 143.6/122.9 (C4,5), 35.1 (NCH_3).

3-Methylbenzoxazolium Tetrafluoroborate (4a).[65] This compound was prepared in the same manner as for **1a** from trimethyloxonium tetrafluoroborate (600 mg, 4.1 mmol) and benzoxazole (507 mg, 4.3 mmol) to afford a white powder (yield: 672 mg, 75%). ^{1}H NMR (d_6-DMSO, 400 MHz): δ 10.57 (s, 1H, C2H), 8.20 (m, 2H, arom CH), 7.85 (m, 2H, arom CH), 4.17 (s, 3H, NCH_3). ^{13}C NMR (d_6-DMSO, 125.76 MHz): δ 158.3 (C2), 148.2/129.0 (C8,9), 129.4/128.2/115.0/113.5 (arom CH), 33.1 (NCH_3).

2-Ethyl-3,4,5-trimethylthiazolium Tetrafluoroborate (1b). ^{1}H NMR (d_6-DMSO, 500 MHz): δ 3.87 (s, 3H, NCH_3), 3.24 (q, 2H, $^3J_{HH}$ = 7.1 Hz ethyl CH_2), 2.46/2.40 (2 × s, 2 × 3H, CCH_3), 1.34 (t, 3H, $^3J_{HH}$ = 7.0 Hz, ethyl CH_3). ^{13}C NMR (d_6-DMSO, 125.76 MHz): δ 173.6 (NCS), 142.0/127.5 (C4,5), 36.9 (NCH_3), 23.1 (ethyl CH_2), 11.7/11.4 (CH_3), 11.6 (ethyl CH_3). MS (ESI): *m*/*z* (%) 156 (100) $[M - BF_4]^+$. Anal. Calcd for $C_8H_{14}NBF_4S$ (243.07): C, 39.53; H, 5.81; N, 5.76. Found: C, 39.56; H, 5.68; N, 5.49.

2-Ethyl-3-methylbenzothiazolium Tetrafluoroborate (2b). ^{1}H NMR (d_6-DMSO, 400 MHz): δ 8.45 (d, 1H, $^3J_{HH}$ = 8.0 Hz, arom CH), 8.31 (d, 1H, $^3J_{HH}$ = 8.4 Hz, arom CH), 7.92 (t, 1H, $^3J_{HH}$ = 7.6 Hz, arom CH), 7.82 (t, 1H, $^3J_{HH}$ = 7.5 Hz, arom CH), 4.22 (s, 3H, NCH_3), 3.49 (q, 2H, $^3J_{HH}$ = 7.2 Hz ethyl, CH_2), 1.48 (t, 3H, $^3J_{HH}$ = 7.3 Hz, ethyl CH_3). ^{13}C NMR (d_6-DMSO, 100.63 MHz): δ 182.9 (NCS), 141.8/128.2 (C8,9), 129.3/127.9/124.3/116.6 (arom CH), 35.9 (NCH_3), 24.1 (ethyl CH_2), 11.5 (ethyl CH_3). MS (ESI): *m*/*z* (%) 178 (100) $[M - BF_4]^+$. Elemental analysis was not satisfactory, due to the hygroscopic nature of this compound.

2-Ethyl-3-methyloxazolium Tetrafluoroborate (3b). ^{1}H NMR (d_6-DMSO, 500 MHz): δ 8.62/8.11 (2 × s, 2 × 1H, C4,5H), 3.81 (s, 3H, NCH_3), 3.15 (q, 2H, $^3J_{HH}$ = 7.4 Hz, ethyl CH_2), 1.31 (t, 3H, $^3J_{HH}$ = 7.4 Hz, ethyl CH_3). ^{13}C NMR (d_6-DMSO, 125.76 MHz): δ 167.6 (NCO), 141.5/123.5 (C4,5), 34.4 (NCH_3), 19.1 (ethyl CH_2), 8.1 (ethyl CH_3). MS (ESI): *m*/*z* (%) 112 (100) $[M - BF_4]^+$. Elemental analysis was not satisfactory, due to the moisture-sensitive nature of this compound.

2-Ethyl-3-methylbenzoxazolium Tetrafluoroborate (4b). ^{1}H NMR (d_6-DMSO, 500 MHz): δ 8.13 (m, 2H, arom CH), 7.79 (m, 2H, arom CH), 4.08 (s, 3H, NCH_3), 3.40 (q, 2H, $^3J_{HH}$ = 7.0 Hz, ethyl CH_2), 1.46 (t, 3H, $^3J_{HH}$ = 7.0 Hz, ethyl CH_3). ^{13}C NMR (d_6-DMSO, 125.76 MHz): δ 171.3 (NCO), 147.2/130.3 (C8,9), 128.4/127.6/114.2/112.8 (arom CH), 32.1 (NCH_3), 20.0 (ethyl CH_2), 8.1 (ethyl CH_3). MS (ESI): *m*/*z* (%) 162 (100) $[M - BF_4]^+$. Elemental analysis was not satisfactory, due to the moisture-sensitive nature of this compound.

3,5-Diethyl-1,4-dimethyl-1,2,4-triazolium Iodide (5b). ^{1}H NMR (d_6-DMSO, 500 MHz): δ 3.98/3.73 (2 × s, 2 × 3H, NCH_3), 3.14 (q, 2H, $^3J_{HH}$ = 7.7 Hz, ethyl CH_2), 2.86 (q, 2H, $^3J_{HH}$ = 7.4 Hz,

(60) Schunn, R. A. *Inorg. Synth.* **1974**, *15*, 5−9.
(61) Smith, V. C. M.; Aplin, R. T.; Brown, J. M.; Hursthouse, M. B.; Karalulov, A. I.; Malik, K. M. A.; Cooley, N. A. *J. Am. Chem. Soc.* **1994**, *116*, 5180−5189.
(62) Chen, Y.-T.; Barletta, G. L.; Haghjoo, K.; Cheng, J. T.; Jordan, F. *J. Org. Chem.* **1994**, *59*, 7714−7722.
(63) Chikashita, H.; Komazawa, S.; Ishimoto, N.; Inoue, K.; Itoh, K. *Bull. Chem. Soc. Jpn.* **1989**, *62*, 1215−1225.
(64) Nakano, T. Jpn. Patent 11,273,733, 1999.
(65) Knecht, J.; Klaus, H.; Grahn, W. *Z. Anorg. Allg. Chem.* **1977**, *32B*, 684−685.

ethyl CH_2), 1.25 (t, 3H, $^3J_{HH} = 7.4$ Hz, ethyl CH_3), 1.20 (t, 3H, $^3J_{HH} = 7.7$ Hz, ethyl CH_3). ^{13}C NMR (d_6-DMSO, 100.63 MHz): δ 155.8/154.4 (C3,5), 37.1/31.5 (NCH_3), 17.6/16.2 (ethyl CH_2), 10.0/9.4 (ethyl CH_3). MS (ESI): *m/z* (%) 154 (100) $[M - I]^+$. Anal. Calcd for $C_8H_{16}N_3I$ (281.14): C, 34.18; H, 5.74; N, 14.95. Found: C, 34.26; H, 5.56; N, 14.80.

Computational Details. Geometry optimizations and harmonic vibrational frequencies for all systems were calculated at the B3LYP[66−68] level of theory with the 6-31G(d) basis set.[69] Zero-point vibrational energy corrections were obtained using unscaled frequencies. All transition structures contained exactly one imaginary frequency and were characterized by following the corresponding normal mode toward the products and reactants.

Higher level single-point energy calculations were performed on all optimized geometries at the B3LYP/6-311+G(2d,p) level of theory.[70−72] Energies from these single-point calculations were combined with the thermodynamic corrections at the lower level of theory to obtain ΔG_{298} values. All energies quoted in this paper refer to these final ΔG_{298} values.

All calculations were performed with the Gaussian 03 set of programs.[73]

Acknowledgment. We are grateful to the EPSRC for funding and the Australian Partnership for Advanced Computing for supercomputing time.

Supporting Information Available: Text, tables, and figures giving complete energy diagrams for each system. This material is available free of charge via the Internet at http://pubs.acs.org.

OM070181E

(66) Hertwig, R. H.; Koch, W. *Chem. Phys. Lett.* **1997**, *268*, 345−351.

(67) Stephens, P. J.; Devlin, J. F.; Chabalowski, C. F.; Frisch, M. J. *J. Phys. Chem.* **1994**, *98*, 11623−11627.

(68) Becke, A. D. *J. Chem. Phys.* **1993**, *98*, 5648−5652.

(69) We initially performed geometry optimizations and corresponding frequency calculations for the $Ni(PPh_3)_2$ and $Ni(P^tBu_3)_2$ systems using the ONIOM method. Following the comment of one of the reviewers, we recalculated these at an all-DFT level. See the Supporting Information for a comparison between results obtained with the ONIOM method and results from the all-DFT calculations.

(70) Frisch, M. J.; Pople, J. A.; Binkley, J. S. **1984**, *80*, 3265−3269.

(71) McLean, A. D.; Chandler, G. S. *J. Chem. Phys.* **1980**, *72*, 5639−5648.

(72) Krishnan, R.; Binkley, J. S.; Seeger, R.; Pople, J. A. *J. Chem. Phys.* **1980**, *72*, 650−654.

(73) Frisch, M. J.; Trucks, G. W.; Schlegel, H. B.; Scuseria, G. E.; Robb, M. A.; Cheeseman, J. R.; Montgomery, J. A., Jr.; Vreven, T.; Kudin, K. N.; Burant, J. C.; Millam, J. M.; Iyengar, S. S.; Tomasi, J.; Barone, V.; Mennucci, B.; Cossi, M.; Scalmani, G.; Rega, N.; Petersson, G. A.; Nakatsuji, H.; Hada, M.; Ehara, M.; Toyota, K.; Fukuda, R.; Hasegawa, J.; Ishida, M.; Nakajima, T.; Honda, Y.; Kitao, O.; Nakai, H.; Klene, M.; Li, X.; Knox, J. E.; Hratchian, H. P.; Cross, J. B.; Bakken, V.; Adamo, C.; Jaramillo, J.; Gomperts, R.; Stratmann, R. E.; Yazyev, O.; Austin, A. J.; Cammi, R.; Pomelli, C.; Ochterski, J. W.; Ayala, P. Y.; Morokuma, K.; Voth, G. A.; Salvador, P.; Dannenberg, J. J.; Zakrzewski, V. G.; Dapprich, S.; Daniels, A. D.; Strain, M. C.; Farkas, O.; Malick, D. K.; Rabuck, A. D.; Raghavachari, K.; Foresman, J. B.; Ortiz, J. V.; Cui, Q.; Baboul, A. G.; Clifford, S.; Cioslowski, J.; Stefanov, B. B.; Liu, G.; Liashenko, A.; Piskorz, P.; Komaromi, I.; Martin, R. L.; Fox, D. J.; Keith, T.; Al-Laham, M. A.; Peng, C. Y.; Nanayakkara, A.; Challacombe, M.; Gill, P. M. W.; Johnson, B.; Chen, W.; Wong, M. W.; Gonzalez, C.; Pople, J. A. *Gaussian 03*, revision C.02; Gaussian, Inc.: Wallingford, CT, 2004.